ACS OMEGA

http://pubs.acs.org/journal/acsodf

Article

Dibenzo[*f,h*]furazano[3,4-*b*]quinoxalines: Synthesis by Intramolecular Cyclization through Direct Transition Metal-Free C−H Functionalization and Electrochemical, Photophysical, and Charge Mobility Characterization

Yuriy A. Kvashnin, Egor V. Verbitskiy,* Oleg S. Eltsov, Pavel A. Slepukhin, Alexey R. Tameev, Natalia V. Nekrasova, Gennady L. Rusinov, Jean-Michel Nunzi, Oleg N. Chupakhin, and Valery N. Charushin

Cite This: *ACS Omega* 2020, 5, 8200−8210

Read Online

ACCESS | Metrics & More | Article Recommendations | Supporting Information

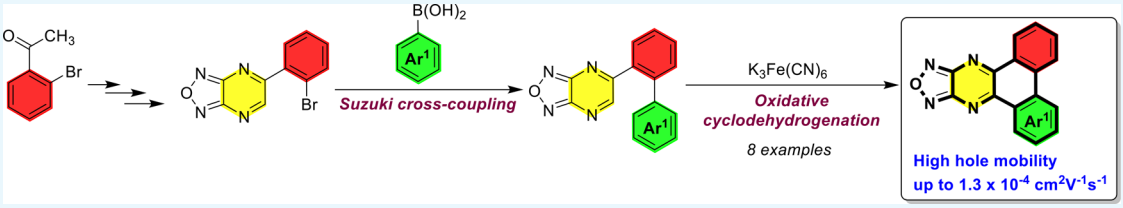

ABSTRACT: Herein, we describe the synthesis of unsymmetrically substituted dibenzo[*f,h*]furazano[3,4-*b*]quinoxalines by intramolecular cyclization through direct transition metal-free C−H functionalization. The electrochemical and photophysical properties for several polycycles have been measured. In thin films of the dibenzo[*f,h*]furazano[3,4-*b*]quinoxalines, hole mobility is in the order of 10^{-4} cm^2 V^{-1} s^{-1}. The results show that the HOMO and LUMO energy levels are appropriate for using the compounds as hole-transport materials in thin-film devices, in particular, organic and perovskite solar cells.

INTRODUCTION

Polycyclic heteroaromatic compounds have received much attention as a fundamental framework in organic functional materials because their electrochemical and photochemical properties are useful in organic electronics and luminescent materials.[1] Among them, 1,4-diazatriphenylene (dibenzo[*f,h*]-quinoxaline) derivatives (**I**) frequently appeared in a molecular unit in the preparation of extended π-conjugated systems with optical characteristic and electrochemical properties (Figure 1).[2] One of the rare azoannulated 1,4-diazatriphenylene derivatives is dibenzo[*f,h*]furazano[3,4-*b*]quinoxaline (**II**). Only two publications reported the synthesis of dibenzo[*f,h*]-furazano[3,4-*b*]quinoxalines (**II**) by condensation of substituted 9,10-phenanthroquinone with 3,4-diaminofurazan under acidic reaction conditions.[3] To the best of our knowledge, there are no synthetic procedures that give the asymmetrically substituted dibenzo[*f,h*]furazano[3,4-*b*]quinoxalines.

We previously reported that 5-(hetero)aryl-[1,2,5]-oxadiazolo[3,4-*b*]pyrazines (**III**) participated in a transition metal-free cross-coupling reactions with different nucleophiles.[4] Therefore, our initial strategy toward dibenzo[*f,h*]-furazano[3,4-*b*]quinoxalines assumed that acid-catalyzed intramolecular cyclization of aryl substituted 5-([1,1′-biphenyl]-2-yl)-[1,2,5]oxadiazolo[3,4-*b*]pyrazines to furnish 9,13-dihydrodibenzo[*f,h*][1,2,5]oxadiazolo[3,4-*b*]quinoxaline intermediates, which could be further oxidized for the synthesis of targets 1,4-diazatriphenylenes (**II**) (Scheme 1).

In this paper, we report a new synthetic protocol for the preparation of unsymmetrically substituted dibenzo[*f,h*]-furazano[3,4-*b*]quinoxalines and their photophysical and electrochemical properties; moreover, we fabricated hole-only devices to measure the hole mobility values in thin films.

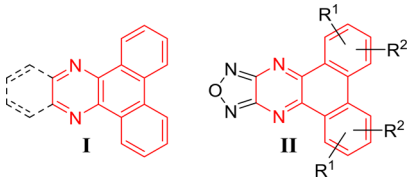

Figure 1. Dibenzo[*f,h*]quinoxaline (**I**) and dibenzo[*f,h*]furazano[3,4-*b*]quinoxaline (**II**) derivatives.

Received: February 3, 2020
Accepted: March 16, 2020
Published: March 30, 2020

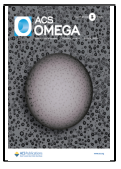

https://dx.doi.org/10.1021/acsomega.0c00479
ACS Omega 2020, 5, 8200−8210

Scheme 1. Interaction of 5-(Hetero)aryl-[1,2,5]oxadiazolo[3,4-*b*]pyrazines with Different Nucleophiles through a Transition Metal-Free Cross-Coupling Reactions

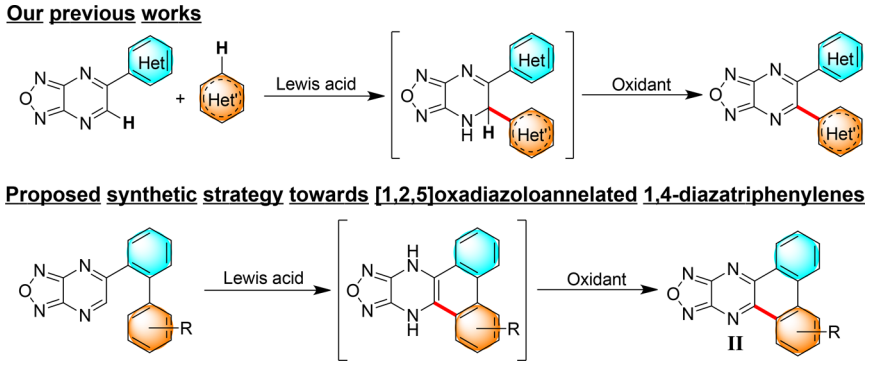

Scheme 2. Synthesis of 5-(2-Bromophenyl)-[1,2,5]oxadiazolo[3,4-*b*]pyrazine (3)

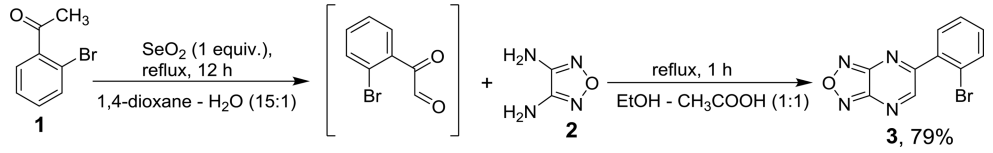

Table 1. Optimization of the Suzuki Cross-Coupling Reaction Conditions

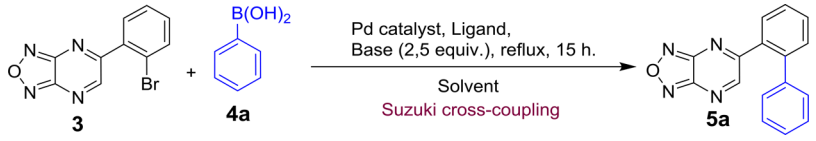

entry	Pd catalyst/ligand (equiv)	base (2.5 equiv)	$PhB(OH)_2$ content (equiv)	solvent	yield (%)
1	$Pd(PPh_3)_4$ (5 mol %)	K_2CO_3	2.0	1,4-dioxane/H_2O (5:1)	16
2	$Pd(PPh_3)_4$ (10 mol %)	K_2CO_3	2.0	1,4-dioxane/H_2O (5:1)	45
3	$Pd(OAc)_2$ (5 mol %)/PPh_3 (10 mol %)	K_3PO_4	2.0	1,4-dioxane	17
4	$Pd(PPh_3)_4$ (5 mol %)	K_3PO_4	1.2	1,4-dioxane	66

RESULTS AND DISCUSSION

Synthesis. At the first stage, the parent 5-(2-bromophenyl)-[1,2,5]oxadiazolo[3,4-*b*]pyrazine (**3**) was obtained via the two-step procedure from readily available 2′-bromoacetophenone (**1**) in 79% overall yield (Scheme 2).

Further, it was necessary to synthesize the series of 5-([1,1′-biphenyl]-2-yl)-[1,2,5]oxadiazolo[3,4-*b*]pyrazine derivatives. 5-(2-Bromophenyl)-[1,2,5]oxadiazolo[3,4-*b*]pyrazine (**3**) reacted with phenylboronic acid (**4a**) to give 5-([1,1′-biphenyl]-2-yl)-[1,2,5]oxadiazolo[3,4-*b*]pyrazine (**5a**) under the Suzuki cross-coupling condition. Examination of the palladium catalysts showed that $Pd(PPh_3)_4$ in dry 1,4-dioxane gave the desired product **5a** in the best yield (Table 1, entry 4).

Based on the above results, the structural diversity of various arylboronic acids (**4a**–**4h**) was examined. As shown in Scheme 3, a wide range of mono-, di-, and trisubstituted phenylboronic acids, bearing both electron-donating and electron-withdrawing substituent groups, could react with **3** for the synthesis of the corresponding 5-bis(aryl)-substituted [1,2,5]oxadiazolo-[3,4-*b*]pyrazines (**5a**–**5h**). As can be seen, the electronic character of the substituents of phenylboronic acids does not have an influence on their reaction activity. In all cases, the Suzuki cross-coupling occurred smoothly to give the desired products **5a**–**5h** in good yields of 51–82% (Scheme 3).

Next, we tried to intramolecular cyclize bis(aryl)-substituted [1,2,5]oxadiazolo[3,4-*b*]pyrazines (**5a**–**5h**) into corresponding

Scheme 3. Synthesis of 5-([1,1′-Biphenyl]-2-yl)-[1,2,5]oxadiazolo[3,4-*b*]pyrazine Derivatives (5a–5h)

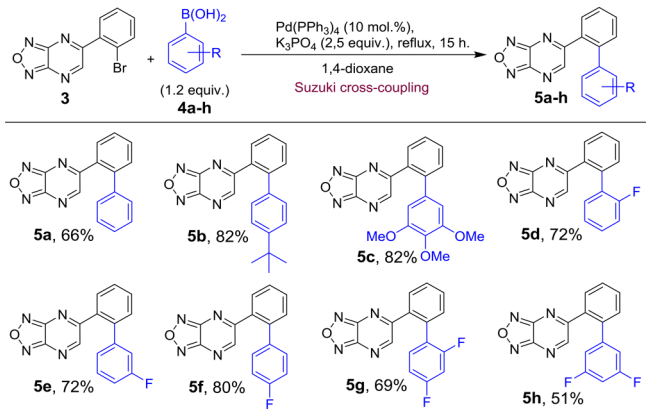

9,13-dihydrodibenzo[*f*,*h*][1,2,5]oxadiazolo[3,4-*b*]quinoxaline by action of CF_3COOH as the best solvent, as shown earlier.[4] The intermediate products **6** were precipitated as white powders in good yields of 56–95%. Notably, compounds **6b** and **6d** were not isolated in their pure forms due to high solubility in CF_3COOH. In these cases, the solvent was removed, and the resulting semisolid residue was oxidized to desired 1,4-diazatriphenylenes **7b** and **7d** without additional purification. Of note, it was found that 2,4-difluoro-9,13-

https://dx.doi.org/10.1021/acsomega.0c00479
ACS Omega 2020, 5, 8200–8210

Scheme 4. Synthesis Dibenzo[*f*,*h*]furazano[3,4-*b*]quinoxaline (DBFQ) Derivatives (7a−7h)

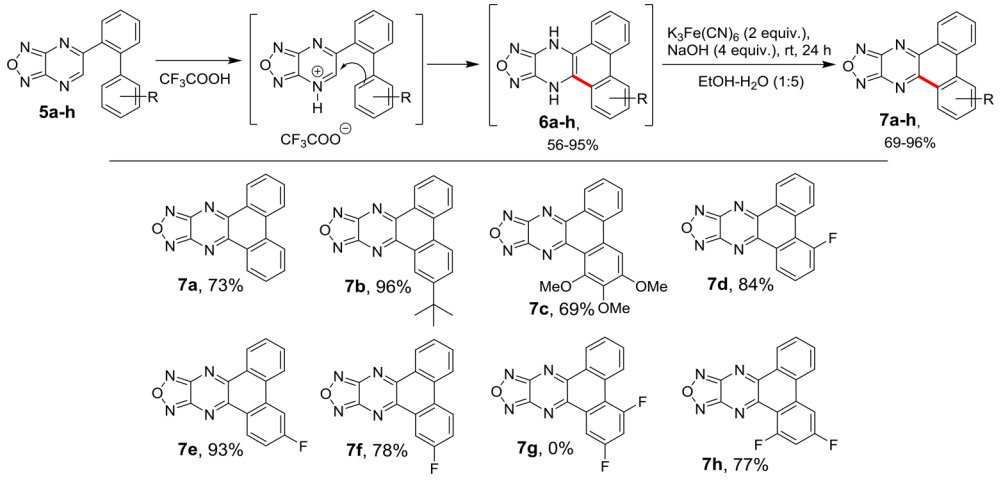

Scheme 5. Structure of Two Possible Regioisomers: 3-Fluorodibenzo[*f*,*h*][1,2,5]oxadiazolo[3,4-*b*]quinoxaline (7e) or 1-Fluorodibenzo[*f*,*h*][1,2,5]oxadiazolo[3,4-*b*]quinoxaline (7e′)

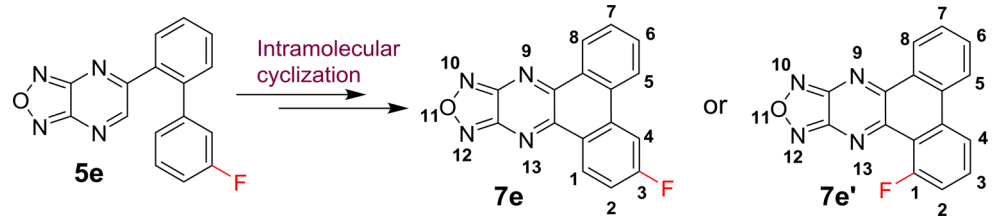

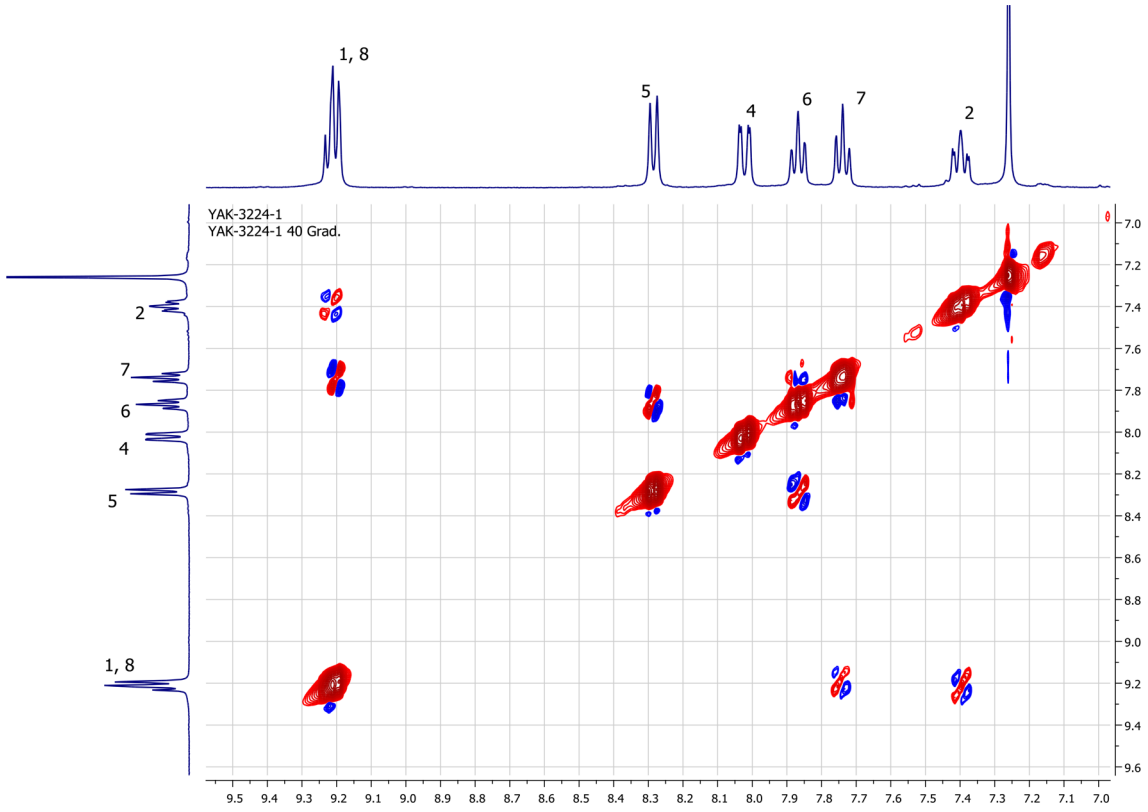

Figure 2. 2D NMR NOESY (400 MHz, $CDCl_3$) spectrum of **7e** at 313 K.

dihydrodibenzo[*f*,*h*][1,2,5]oxadiazolo[3,4-*b*]quinoxaline (**6g**) is not formed under the given reaction conditions. We suggest that it is due to the uncoordinated electron-withdrawing inductive effect of two fluorine atoms, which complicate the intramolecular electrophilic attack on the 1,1′-biphenyl substituents. The obtained 9,13-dihydrodibenzo[*f*,*h*][1,2,5]-

https://dx.doi.org/10.1021/acsomega.0c00479
ACS Omega 2020, 5, 8200−8210

oxadiazolo[3,4-*b*]quinoxalines (**6a**−**6f** and **6h**) were oxidized with $K_3Fe(CN)_6$ in an alcohol solution (NaOH) for 24 h to afford target dibenzo[*f*,*h*]furazano[3,4-*b*]quinoxalines (**7a**−**7f** and **7h**) in high yields of 69−96% (Scheme 4).

At the cyclization of the compound **5e**, the formation of two regioisomeric products, which differ at the C(1) or C(3) position of the fluorine atom, is possible (Scheme 5). To unambiguously confirm the structure of the polycyclic compound **7e** or **7e′**, two-dimensional NOESY spectrum was recorded for this compound (Figure 2). Particularly, for the proposed structure of **7e′** in the NOESY spectrum, cross-peaks due to spatial interactions of the protons H(2), H(3), and H(4) forming the common system should be expected. Besides, the interactions with neighboring protons H(2) and H(4) should be observed for proton H(3). However, no cross-peaks with any of the neighboring protons were detected for proton H(4) in the NOESY experiment. Furthermore, for the other protons of the aromatic system H(1) and H(2), the interactions only with each other have been observed. This evidence unambiguously supports the structure of **7e**.

Notably, the structure of **7h** was established by X-ray diffraction analysis (Figure 3). According to the XRD data,

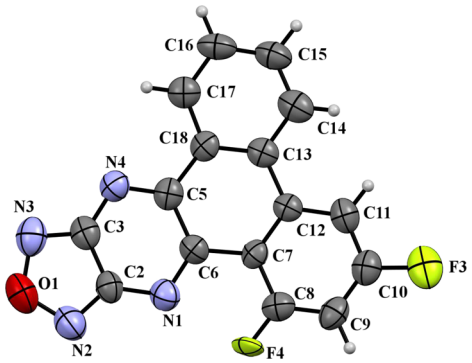

Figure 3. ORTEP of **7h** with thermal ellipsoids at the 50% probability level.

compound **7h** crystallized in the noncentrosymmetric space group. The polycyclic system is planar (Figure 3). The fluoroaryl fragment is disordered in the plane with an occupancy coefficient of 0.85/0.15. The mean bond distances and angles of the molecules are near to standard. In the crystal, the molecules form the twisted slanting stacks (Figure 4a−c), with interfacial distances of adjacent molecules being approximately 3.3 Å (Figure 4d), which is near the layer distance in graphite (3.35 Å).[5] This is a characteristic for a pronounced $\pi-\pi$ interaction between two aromatic cores. These results suggest that the other analogue polycycles **7a** and **7c**−**7f** without the bulky propping *tert*-butyl group also may hold strong intermolecular $\pi-\pi$ stacking interactions. In fact, relatively poor solubility was observed for **7d**, **7e**, and **7h**, which reflects the strong $\pi-\pi$ interactions.[6]

Optical and Photophysical Properties. The electrochemical properties of dibenzo[*f*,*h*]furazano[3,4-*b*]-quinoxalines (**7a**−**7f** and **7h**) were studied using cyclic voltammetry under conditions previously described for similar heteroacene systems.[7] The cyclic voltammograms shown in Figures S1−S7 demonstrate the irreversible character of the reduction of compounds **7a**−**7f** and **7h**. Given that no anodic behavior of 1,4-diazatriphenylenes (**7a**−**f** and **h**) could be recorded by CV, their excited state oxidation potentials (corresponding to the HOMO energy levels) were calculated by subtracting the optical energy gap E_g^{opt} (estimated from the long-wavelength absorption edge of the absorption spectra[8] recorded in CH_2Cl_2 solution shown in Figures S8−S14) from the LUMO energy values (Table 2). The compounds under study are considered to be used in the solid state, so the similar optical and electrochemical parameters, as well as hole mobility (Table 2), were measured in their thin solid films (see Experimental Section). Both HOMO and LUMO energy levels of the compounds in solution are downshifted compared with those in solid films because of the influence of the reorganization energy of the electrolyte on the dispersion of the energy level of the substance in solution.

Computational Data. The DFT calculations of the HOMO levels and the energy gap, as well as the dipole moment of molecules in the neutral state, were done at the B3LYP/6-31G* level of theory in vacuum.[9] The computational data are shown in Table 2. The results show that the HOMO and LUMO levels were uniformly overestimated in the DFT calculations, presumably because the calculations were performed in a vacuum. The calculated band gap energies E_g^{calc} are systematically higher than the experimental E_g^{opt} values.

Hole Mobility. Organic semiconductors that can potentially be used as a charge-transporting material must possess reasonable charge carrier mobility values. Thus, we prepared specimens of a diode structure ITO/SiO_2/ DBFQ/Au where the SiO_2 insulator layer blocked injection of charge carriers from the ITO electrode in CELIV measurements (see Experimental Section). The data on hole mobility in the solid films of dibenzo[*f*,*h*]furazano[3,4-*b*]quinoxalines are also summarized in Table 2. The hole mobility in the **7a**, **7d**, and **7e** films is 2.5−6 times larger than that in the **7b**, **7c**, **7f**, and **7h** films.

The charge carrier transport in organic and polymer solids can be represented in terms of the redox process.[10−13] The hole transport is considered as a chain of redox reactions, consisting of one electron transfer from the HOMO of the neutral molecules to the single occupied molecular orbital (SOMO) of the neighbor radical cations. When the neutral molecule is charged positively, its conformation is transformed to accommodate the minimum energy state of the radical cation. In turn, when the SOMO of the radical cation accepts the second electron, its conformation is also transformed. Evidently, such molecule reorganization influences the probability of the intermolecular electron transfer and, as a consequence, the mobility of charge carriers. Indeed, molecule **7a** consists of a solid core backbone, whereas other molecules have substituents, which can cause molecule conformation transformations during charge transfer. The fluorine substituent in the **7d** and **7e** molecules seems to initiate negligible transformations between the charged and neutral states of the molecules, so the high hole mobility for their films obeys the suggested approach as well.

It is understood that the packing of the molecules in solid films influences the charge carrier transport. As was discussed above, **7a** and **7c**−**7h** molecules tend to form strong intermolecular $\pi-\pi$ stacking interactions. In consequence, we can expect relatively high charge mobility in their films in accordance with the fact that charge transport along the axis of such stack is faster than in any other direction.[13] Nevertheless, the hole mobility in the **7c**, **7f**, and **7h** films is lower than that

https://dx.doi.org/10.1021/acsomega.0c00479
ACS Omega 2020, 5, 8200−8210

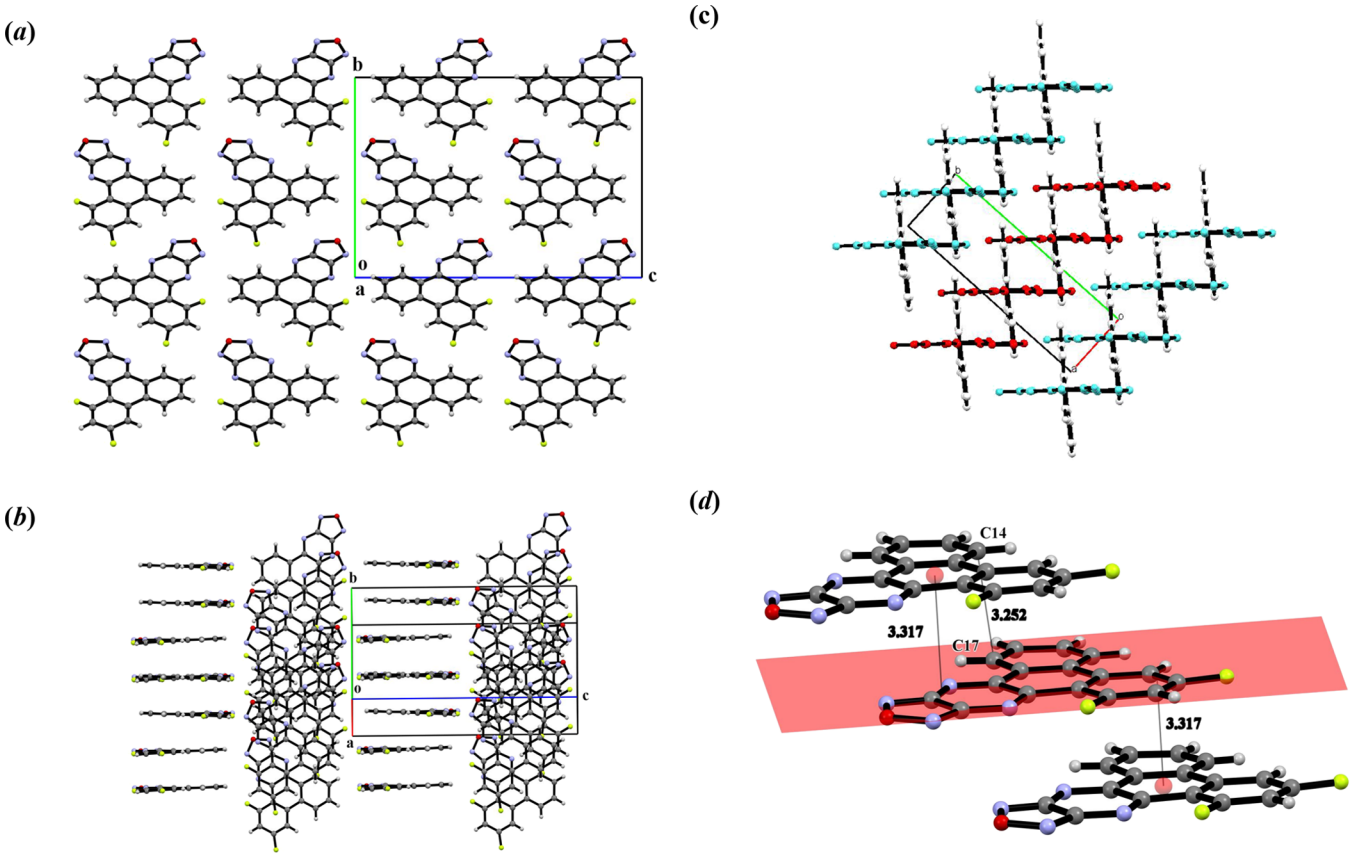

Figure 4. Molecular packing for **7h** (a) in the plane [100], (b) along the plane [8 24 0], and (c) in the plane [001]. (d) Fragment of stack with interfacial distances in Å.

in the **7a**, **7d**, and **7e** films. In this regard, the dipole nature of the bulk of the films may be taken into account as well.[14,15]

In accordance with the well-developed correlated disorder model (CDM),[15] considering the Gaussian distribution of density of states, the following relationship describes charge mobility (see eq 1)

$$\mu = \mu_0 \exp\left[\left(\frac{3\sigma}{5kT}\right)^2 + C_0\left(\left(\frac{\sigma}{kT}\right)^{3/2} - \Gamma\right)\left(\frac{eRF}{\sigma}\right)^{1/2}\right] \quad (1)$$

where $C_0 = 0.78$, $\Gamma = 2$, μ_0 is the pre-exponential factor, R is the distance between charge transport sites, F is the applied electric field, e is the electron charge, k is the Boltzmann constant, T is the temperature, and σ is the root mean square width of the energetic disorder. In general, the latter is determined by a dipolar component, σ_d, a van der Waals component, σ_v, and a quadrupolar component, σ_q, so as $\sigma^2 = \sigma_d^2 + \sigma_v^2 + \sigma_q^2$. To a quite good approximation, the contribution of the van der Waals and quadrupolar components may be neglected in comparison with the dipolar component, which is given by $\sigma_d = 2.35ep/(\varepsilon R)$ where p is the dipole moment of the transport molecule and ε is the permanent dielectric constant of the medium. It is seen that the lower the molecule dipole moment, the lower the amplitude of disorder and hence the larger the charge carrier mobility in the solid film. This correlation is revealed for **7d** and **7e** molecules, possessing the lower dipole moment compared with the **7c**, **7f**, and **7h** molecules (Table 2). Meanwhile, the correlation fails if **7a** molecules are compared to the **7b**, **7f**, and **7h** molecules, with the molecules possess a similar dipole moment. It means that the CDM does not apply to the **7a** films. We may suppose that the degree of ordering (stacking) of the **7a** molecules in the film formed on a glass/ITO/SiO_2 substrate is higher than that of the **7b**, **7f**, and **7h** molecules.

CONCLUSIONS

In summary, we have developed a new approach for the synthesis of unsymmetrical dibenzo[*f*,*h*]furazano[3,4-*b*]-quinoxalines via intramolecular oxidative cyclodehydrogenation of the corresponding 5-phenylaryl(hetaryl)-substituted [1,2,5]oxadiazolo[3,4-*b*]pyrazines. The present synthetic procedure provides a facile way to the family of nitrogen-containing polycyclic heteroaromatic compounds that can potentially be used in organic electronics and luminescent materials.

Namely, we observed that a compromise between molecule stiffness, molecule dipole moment, and intermolecular packaging defines the mobility of holes in the solid films of the dibenzo[*f*,*h*]furazano[3,4-*b*]quinoxalines. In the films, hole mobility in the order of 10^{-4} cm^2 V^{-1} s^{-1} was experimentally measured, which makes the compounds promising hole-transporting materials for organic electronics. In particular, **7b**−**7h** compounds are promising candidates for the hole-transport layer in perovskite solar cells. Under similar conditions, the CELIV mobility of the pristine staple-compound Spiro-MeOTAD,[16] which is commonly used as the hole-transport layer, was 8.5×10^{-7} cm^{-2} V^{-1} s^{-1} (for comparison, the hole mobility obtained from space charge limited current and time-of-flight measurements reached 2 ×

https://dx.doi.org/10.1021/acsomega.0c00479
ACS Omega 2020, 5, 8200−8210

Table 2. Optical, Electrochemical, and Hole Mobility Data for Dibenzo[*f*,*h*]furazano[3,4-*b*]quinoxalines

compound	E_{red}^{onset}[a] (V)	E_{HOMO}[b]/E_{HOMO}[c] (eV)	E_{LUMO}[b,d]/E_{LUMO}[c,d] (eV)	E_g^{opt}[b]/E_g^{opt}[c] (±0.03 eV)	Absorption[b] λ_{max} (nm)/ε (10^3 M^{-1} cm^{-1})	hole mobility[c] (10^{-5} cm^2 V^{-1} s^{-1}) (CI[e] 95%)	dipole moment[f] (D)
7a	−0.81	−7.15/−5.61	−4.29/−3.01	2.86/2.60	387/12.95 305/21.35 294/13.52 267/19.20	12.7 ± 1.5	6.81
7b	−0.83	−7.12/−5.23	−4.27/−2.68	2.85/2.55	389/14.21 308/21.46 297/15.73 275/25.02	2.5 ± 0.5	6.87
7c	−0.93	−6.74/−5.24	−4.17/−3.04	2.57/2.20	412/13.80 311/15.98 279/29.98 253/49.20	5.1 ± 0.4	8.62
7d	−0.75	−7.11/−5.23	−4.35/−2.99	2.76/2.24	395/12.43 304/20.16 293/12.97	16.0 ± 4.0	5.43
7e	−0.80	−7.16/−5.27	−4.30/−2.72	2.86/2.55	386/14.73 303/20.52 292/13.24 275/22.76	13.3 ± 1.6	5.57
7f	−0.75	−7.25/−5.25	−4.35/−2.80	2.90/2.45	384/11.85 307/26.34 296/16.82 271/18.09	2.4 ± 0.4	6.77
7h	−0.78	−7.18/−5.27	−4.32/−2.87	2.87/2.40	384/14.54 301/16.47 290/11.49 267/21.02	3.5 ± 1.6	6.57

[a] E_{red}^{onset}, onset of reduction potential (vs Ag/AgCl reference electrode). [b] Parameters measured in solutions at room temperature at $C = 1.0 \times 10^{-5}$ M (for optical) and $C = 5.0 \times 10^{-3}$ M (for electrochemical). [c] Parameters measured for solid films at room temperature. [d] $E_{LUMO} = E_{HOMO} - E_g^{opt}$. [e] Confidence interval calculated from 10 replicates. [f] DFT calculation data.

10^{-4} cm^{-2} V^{-1} s^{-1} at high field).[17] Moreover, their HOMO levels match well with those of $MAPbI_3$ and $MAPbBr_3$ hybrid perovskites.

EXPERIMENTAL SECTION

All reagents and solvents were obtained from commercial sources and dried by using standard procedures before use.

^1H and ^{13}C NMR spectra were recorded on AVANCE 500 and AVANCE II 400 MHz instruments using Me_4Si as an internal standard. Elemental analysis was carried on a Eurovector EA 3000 automated analyzer. Melting points were determined on Boetius combined heating stages and were not corrected.

Flash column chromatography was carried out using Alfa Aesar silica gel 0.040−0.063 mm (230−400 mesh), eluting with ethyl acetate/hexane. The progress of reactions and the purity of compounds were checked by TLC on Sorbfil plates (Russia) in which the spots were visualized with UV light (λ, 254 or 365 nm).

The XRD experiment was performed on an Xcalibur 3 diffractometer on the standard procedure (MoK irradiation, graphite monochromator, ω scans with 1° step at $T = 295(2)$ K). Empirical absorption correction was applied. Using Olex2,[18] the structure was solved with the Superflip[19] structure solution program using charge flipping and refined with the olex2.refine refinement package using Gauss−Newton minimization. All nonhydrogen atoms were refined in anisotropic approximation; H atoms were refined isotropically in the "rider" model. The mean crystallographic data and results of the refinements are presented in Table S1. The X-ray crystallography data for the structure reported in this paper have been deposited with Cambridge Crystallography Data Centre as supplementary publications CCDC 1976356 for **7h**. These data can be obtained free of charge from the Cambridge Crystallographic Data Centre via www.ccdc.cam.ac.uk/data_request/cif.

Cyclic voltammetry was carried out on a Metrohm Autolab PGSTAT128N potentiostat with a standard three-electrode configuration. Typically, a three-electrode cell equipped with a platinum working electrode, a $Ag/AgNO_3$ (0.01 M) reference electrode, and a glass carbon rod counter electrode was employed. The measurements were done in dichloromethane solution, containing the present compound (5×10^{-3} M) with tetrabutylammonium perchlorate (0.1 M) as the supporting electrolyte under an argon atmosphere at a scan rate of 100 mV s^{-1}. The potential of the reference electrode was calibrated by using the ferrocene/ferrocenium redox couple (Fc/Fc^+), which has a known oxidation potential of +5.1 eV versus vacuum for ferrocene.[20] After calibration of the measurements against Fc/Fc^+, the HOMO energy level was calculated according to the following equation (eq 2)

$$E_{HOMO}\ (eV) = -[E_{ox}^{onset} - E_{1/2}(Fc/Fc^+) + 5.1] \quad (2)$$

where $E_{1/2}(Fc/Fc^+)$ is the half-wave potential of the Fc/Fc^+ couple (the oxidation potential of which is assumed at 5.1 eV) against the Ag/Ag^+ electrode.

https://dx.doi.org/10.1021/acsomega.0c00479
ACS Omega 2020, 5, 8200−8210

UV−vis spectra were recorded for a 1×10^{-5} M dichloromethane solution with a Shimadzu UV-2401PC spectrophotometer.

Since some of the dibenzo[*f*,*h*]furazano[3,4-*b*]quinoxaline derivatives under study were poor soluble, their thin solid films were prepared by thermal evaporation in vacuum. The morphology of the film was not studied. In thin layers of the dibenzo[*f*,*h*]furazano[3,4-*b*]quinoxaline derivatives, HOMO−LUMO energy levels were determined by cyclic voltammetry (CV). The CV experiment was carried out at a scan rate of 20 mV s^{-1} in a three-electrode, three-compartment electrochemical cell in the glovebox with a dry argon atmosphere. Platinum sheets served as working and counter electrodes. A 20 nm solid layer of an examined material was preliminarily deposited onto the working electrode by thermal evaporation of the compound under 10^{-6} mbar vacuum at a rate of 1 Å s^{-1}. A 0.2 M solution of tetrabutylammonium hexafluorophosphate (NBu_4PF_6, Fluka) in acetonitrile (MeCN (Aldrich, HPLC-grade)) was used as an electrolyte. The electrolyte solution was prepared as follows. To remove impurities and traces of water, MeCN was stirred with calcium hydride (10 g L^{-1}) for 2 days, fractionally distilled with P_2O_5 (5 g L^{-1}), then heated near the boiling point for 2 h with CaH_2 (5 g L^{-1}), and finally fractionally distilled again. NBu_4PF_6 was purified by recrystallization in ethanol and then dried and heated for 4 h at 80 °C in the inert dry argon atmosphere in the glovebox. The electrolyte solution was prepared in the glovebox also. A Ag wire immersed into the electrolyte solution with the addition of 0.1 M $AgNO_3$ was used as a pseudo reference electrode (Ag/Ag^+). It was calibrated against ferrocene/ferrocenium couple (−0.039 V vs Ag/Ag^+), and its potential was recalculated to the energy scale using a value of −4.988 eV for Fc/Fc^+ in MeCN reported in the literature.[21] Thus, the energy level of Ag/Ag^+ ($E_{Ag/Ag+}$) in this case is −5.027 eV. Considering the accuracy of CVA experiment (±0.02 V), this value should be rounded to −5.03 eV.

A 20 nm solid film of an examined material was deposited onto the working electrode by thermal evaporation of the compound under 10^{-6} mbar vacuum at a rate of 1 Å s^{-1}. The values of potentials corresponding to the HOMO levels were determined by applying a tangent to the onset of anodic and cathodic currents, followed by extrapolation of the tangent to zero current at the crossing with the axis of potentials. For all the substances, we failed to determine the LUMO level because of the rather wide optical band gap ranged around 2.4−2.6 eV. Therefore, considering the determined electrochemical response of HOMO, the response of LUMO should lay in the range of potentials near −2.4 V, which is close to the cathodic limit of the electrochemical stability window of MeCN.

Charge Carrier Mobility Measurements. In thin solid films, the charge mobility values were measured by using the technique of charge extraction by linearly increasing voltage (CELIV).[22] Metal−insulator−semiconductor (MIS) diode structures, similar to those described in references,[23,24] were prepared.

Onto the ITO (indium tin oxide) electrode of the ITO/glass substrate, a SiO_2 insulator layer of 70 nm in thickness was deposited by conventional magnetron sputtering. Then, a 100 nm layer of the dibenzo[*f*,*h*]furazano[3,4-*b*]quinoxaline derivative and an 80 nm layer of the Au electrode were deposited successively by thermal evaporation of the material under 10^{-6} mbar vacuum at a rate of 1 Å s^{-1}.

For CELIV measurements, an arbitrary waveform generator and oscilloscope (DLAnalog Discovery with WaveForms software) were used to generate the triangle voltage pulse with a proper ramp and offset. CELIV signals were recorded by a digital storage oscilloscope (Tektronix TDS3032B) as well. The charge carrier mobility μ was determined in accordance with eq 3[22]

$$\mu = \frac{2d^2}{3At_{max}^2\left[1 + \frac{0.36\Delta j}{j(0)}\right]} \quad (3)$$

where d is the film thickness, A is the applied voltage ramp, $j(0)$ is the displacement current, and Δj is the maximum drift current at "t_{max}". The latter three parameters were extracted from CELIV transient current curves.

Synthesis of 5-(2-Bromophenyl)-[1,2,5]oxadiazolo-[3,4-*b*]pyrazine (3). Selenium dioxide (1.1 g, 10 mmol) was dissolved in 1,4-dioxane/H_2O (15:1, 16 mL), and the mixture was heated and refluxed for 5 min. 2′-Bromoacetophenone (**1**) (1.99 g, 10 mmol) was added, and heating was continued for the next 12 h. The reaction mixture was filtered, and the filtrate was concentrated under reduced pressure to give 2-bromophenylglyoxal as a light yellow oil. The solution of 3,4-diaminofurazan (**2**) (1.0 g, 10 mmol) and crude 2-bromophenylglyoxal in a mixture of EtOH (5 mL) and CH_3COOH (5 mL) was refluxed for 1 h. After that, the mixture was cooled down, and the precipitate was filtered off, washed with ethanol, and then air-dried. The desired product **3** was obtained as a crystalline yellow powder. Yield: 2.19 g, 79%. mp 135 °C. ^{1}H NMR (500 MHz, DMSO-d_6): δ 9.44 (s, 1H), 7.91 (dd, J = 8.0, 1.1 Hz, 1H), 7.79 (dd, J = 7.6, 1.7 Hz, 1H), 7.68 (td, J = 7.6, 1.1 Hz, 1H), 7.63−7.59 (m, 1H). ^{13}C NMR (126 MHz, DMSO-d_6): δ 162.4, 157.1, 151.9, 151.1, 136.1, 133.4, 133.1, 132.4, 128.5, 121.0. Calcd for $C_{10}H_5BrN_4O$ (277.08): C, 43.35; H, 1.87; N, 20.22. Found: C, 43.41; H, 1.84; N, 20.10.

General Procedure for the Synthesis of 5-([1,1′-Biphenyl]-2-yl)-[1,2,5]oxadiazolo[3,4-*b*]pyrazine Derivatives (5a−5h). A mixture of 5-(2-bromophenyl)-[1,2,5]-oxadiazolo[3,4-*b*]pyrazine (**1**) (277 mg, 1.0 mmol), corresponding arylboronic acids **4a−4h** (1.2 mmol), $Pd(PPh_3)_4$ (115 mg, 10 mol %), and K_3PO_3 (530 mg, 2.5 mmol) was dissolved in 1,4-dioxane (15 mL). The reaction mixture was degassed and refluxed for 15 h under an argon atmosphere. After completion of the reaction (monitored by TLC), 10 mL of water was added and extracted with ethyl acetate. The combined organic layer was washed with water and brine, dried over anhydrous Na_2SO_4, and concentrated in vacuo. Purification by silica gel column chromatography with ethyl CH_2Cl_2/hexane (1:2, v/v) as an eluent and recrystallization from EtOH were performed to afford the title compounds (**5a−5h**).

*5-([1,1′-Biphenyl]-2-yl)-[1,2,5]oxadiazolo[3,4-b]pyrazine (**5a**).* Yield: 182 mg, 66%, pale yellow powder. mp 143 °C. ^{1}H NMR (400 MHz, DMSO-d_6): δ 8.25 (s, 1H), 7.93 (dd, J = 8.0, 1.2 Hz, 1H), 7.81−7.77 (m, 1H), 7.71−7.67 (m, 2H), 7.40−7.36 (m, 3H), 7.32−7.27 (m, 2H). ^{13}C NMR (101 MHz, DMSO-d_6): δ 163.9, 156.6, 152.2, 150.7, 141.2, 139.0, 134.1, 132.0, 131.5, 130.5, 129.9, 129.1, 128.34, 128.32. Calcd for $C_{16}H_{10}N_4O$ (274.28): C, 70.06; H, 3.68; N, 20.43. Found: C, 70.03; H, 3.74; N, 20.36.

https://dx.doi.org/10.1021/acsomega.0c00479
ACS Omega 2020, 5, 8200−8210

*5-(4′-tert-Butyl-[1,1′-biphenyl]-2-yl)-[1,2,5]oxadiazolo-[3,4-b]pyrazine (**5b**).* Yield: 270 mg, 82%, pale yellow powder. mp 142 °C. ^{1}H NMR (400 MHz, DMSO-d_6): δ 8.24 (s, 1H), 7.91 (d, J = 7.8 Hz, 1H), 7.80−7.75 (m, 1H), 7.70−7.64 (m, 2H), 7.41 (d, J = 7.9 Hz, 2H), 7.23 (d, J = 7.9 Hz, 2H), 1.28 (s, 9H). ^{13}C NMR (101 MHz, DMSO-d_6): δ 164.0, 156.6, 152.3, 151.0, 150.7, 141.1, 136.1, 134.0, 132.0, 131.5, 130.5, 129.6, 128.2, 125.9, 34.3, 31.0. Calcd for $C_{20}H_{18}N_4O$ (330.39): C, 72.71; H, 5.49; N, 16.96. Found: C, 72.51; H, 5.40; N, 17.18.

*5-(3′,4′,5′-Trimethoxy-[1,1′-biphenyl]-2-yl)-[1,2,5]-oxadiazolo[3,4-b]pyrazine (**5c**).* Yield: 298 mg, 82%, orange powder. mp 154 °C. ^{1}H NMR (500 MHz, DMSO-d_6): δ 8.30 (s, 1H), 7.92 (d, J = 7.6 Hz, 1H), 7.80−7.72 (m, 2H), 7.70−7.66 (m, 1H), 6.52 (s, 2H), 3.67 (s, 3H), 3.58 (s, 6H). ^{13}C NMR (126 MHz, DMSO-d_6): δ 164.1, 156.8, 153.2, 152.1, 150.5, 141.3, 137.7, 134.6, 134.0, 132.0, 131.3, 130.3, 128.3, 107.6, 60.1, 55.9. Calcd for $C_{19}H_{16}N_4O_4$ (364.36): C, 62.63; H, 4.43; N, 15.38. Found: C, 62.43; H, 3.53; N, 15.26.

*5-(2′-Fluoro-[1,1′-biphenyl]-2-yl)-[1,2,5]oxadiazolo[3,4-b]pyrazine (**5d**).* Yield: 210 mg, 72%, pale yellow powder. mp 151 °C. ^{1}H NMR (500 MHz, DMSO-d_6): δ 8.75 (s, 1H), 7.98 (dd, J = 7.7, 1.0 Hz, 1H), 7.80 (td, J = 7.6, 1.3 Hz, 1H), 7.73 (td, J = 7.6, 1.1 Hz, 1H), 7.65 (d, J = 7.6 Hz, 1H), 7.46−7.39 (m, 2H), 7.26 (td, J = 7.6, 0.8 Hz, 1H), 7.18−7.13 (m, 1H). ^{13}C NMR (126 MHz, DMSO-d_6): δ 162.9, 158.4 (d, $^{1}J_{C,F}$ = 245.1 Hz), 156.5, 151.8, 150.7, 134.8 (d, $^{4}J_{C,F}$ = 4.8 Hz), 132.2 (d, $^{4}J_{C,F}$ = 2.8 Hz), 131.8, 131.5, 130.9, 130.8 (d, $^{3}J_{C,F}$ = 8.4 Hz), 128.9, 126.6, 126.5, 125.2 (d, $^{4}J_{C,F}$ = 3.5 Hz), 115.9 (d, $^{2}J_{C,F}$ = 22.1 Hz). ^{19}F NMR (471 MHz, DMSO-d_6): δ 45.87 (ddd, J = 10.6, 7.7, 5.4 Hz) ppm. Calcd for $C_{16}H_9FN_4O$ (292.27): C, 65.75; H, 3.10; N, 19.17. Found: C, 65.70; H, 3.05; N, 19.24.

*5-(3′-Fluoro-[1,1′-biphenyl]-2-yl)-[1,2,5]oxadiazolo[3,4-b]pyrazine (**5e**).* Yield: 210 mg, 72%, pale yellow powder. mp 153 °C. ^{1}H NMR (500 MHz, DMSO-d_6): δ 8.42 (s, 1H), 7.94 (dd, J = 7.6, 0.9 Hz, 1H), 7.79 (td, J = 7.5, 1.3 Hz, 1H), 7.71 (ddd, J = 9.9, 5.6, 1.7 Hz, 2H), 7.35 (td, J = 7.9, 6.3 Hz, 1H), 7.32−7.28 (m, 1H), 7.24 (td, J = 8.4, 2.1 Hz, 1H), 6.99 (d, J = 7.8 Hz, 1H). ^{13}C NMR (126 MHz, DMSO-d_6): δ 163.3, 162.3 (d, $^{1}J_{C,F}$ = 245.4 Hz), 156.7, 152.2, 150.7, 141.4 (d, $^{3}J_{C,F}$ = 7.9 Hz), 139.9 (d, $^{4}J_{C,F}$ = 2.1 Hz), 134.4, 132.0, 131.6, 130.9 (d, $^{3}J_{C,F}$ = 8.6 Hz), 130.7, 128.8, 126.5 (d, $^{4}J_{C,F}$ = 2.7 Hz), 116.4 (d, $^{2}J_{C,F}$ = 22.0 Hz), 115.2 (d, $^{3}J_{C,F}$ = 21.0 Hz). ^{19}F NMR (471 MHz, DMSO-d_6): δ 50.83−50.78 (m). Calcd for $C_{16}H_9FN_4O$ (292.27): C, 65.75; H, 3.10; N, 19.17. Found: C, 65.68; H, 3.17; N, 19.35.

*5-(4′-Fluoro-[1,1′-biphenyl]-2-yl)-[1,2,5]oxadiazolo[3,4-b]pyrazine (**5f**).* Yield: 232 mg, 80%, pale yellow powder. mp 151 °C. ^{1}H NMR (500 MHz, DMSO-d_6): δ 8.35 (s, 1H), 7.92 (dd, J = 7.6, 0.8 Hz, 1H), 7.78 (td, J = 7.6, 1.2 Hz, 1H), 7.70−7.65 (m, 2H), 7.36−7.32 (m, 2H), 7.23−7.17 (m, 2H). ^{13}C NMR (126 MHz, DMSO-d_6): δ 163.6, 162.07 (d, $^{1}J_{C,F}$ = 246.3 Hz), 156.7, 152.2, 150.7, 140.2, 135.4 (d, $^{4}J_{C,F}$ = 3.0 Hz), 134.1, 132.1, 132.0 (d, $^{4}J_{C,F}$ = 3.8 Hz), 131.5, 130.6, 128.4, 116.0 (d, $^{2}J_{C,F}$ = 21.6 Hz). ^{19}F NMR (471 MHz, DMSO-d_6): δ 48.91 (dq, J = 8.9, 5.4 Hz). Calcd for $C_{16}H_9FN_4O$ (292.27): C, 65.75; H, 3.10; N, 19.17. Found: C, 65.63; H, 3.04; N, 19.17.

*5-(2′,4′-Difluoro-[1,1′-biphenyl]-2-yl)-[1,2,5]oxadiazolo-[3,4-b]pyrazine (**5g**).* Yield: 214 mg, 69%, yellow powder. mp 141 °C. ^{1}H NMR (500 MHz, DMSO-d_6): δ 8.86 (s, 1H), 7.99 (dd, J = 7.7, 1.2 Hz, 1H), 7.80 (td, J = 7.6, 1.4 Hz, 1H), 7.74 (td, J = 7.6, 1.3 Hz, 1H), 7.63 (d, J = 7.6 Hz, 1H), 7.47 (td, J = 8.7, 6.6 Hz, 1H), 7.22 (ddd, J = 10.6, 9.4, 2.5 Hz, 1H), 7.15 (td, J = 8.4, 2.3 Hz, 1H). ^{13}C NMR (126 MHz, DMSO-d_6): δ 162.6, 162.2 (dd, $^{1}J_{C,F}$ = 248.2, $^{3}J_{C,F}$ = 12.3 Hz), 158.5 (dd, $^{1}J_{C,F}$ = 247.7, $^{3}J_{C,F}$ = 12.6 Hz), 156.5, 151.7, 150.7, 134.7, 134.0, 133.3 (dd, $^{3}J_{C,F}$ = 9.8, $^{4}J_{C,F}$ = 4.3 Hz), 131.8, 131.5, 130.9, 129.9 (d, $^{1}J_{C,F}$ = 240.1 Hz), 123.2 (dd, $^{2}J_{C,F}$ = 15.0, $^{4}J_{C,F}$ = 3.8 Hz), 112.3 (dd, $^{2}J_{C,F}$ = 21.3, $^{4}J_{C,F}$ = 3.6 Hz), 104.3 (t, $^{2}J_{C,F}$ = 26.4 Hz). ^{19}F NMR (471 MHz, DMSO-d_6): δ 53.22−53.15 (m, 1F), 50.70 (dd, J = 18.8, 8.9 Hz, 1F). Calcd for $C_{16}H_8F_2N_4O$ (310.26): C, 61.94; H, 2.60; N, 18.06. Found: C, 61.91; H, 2.70; N, 18.26.

*5-(3′,5′-Difluoro-[1,1′-biphenyl]-2-yl)-[1,2,5]oxadiazolo-[3,4-b]pyrazine (**5h**).* Yield: 160 mg, 51%, yellow powder. mp 124 °C. ^{1}H NMR (400 MHz, DMSO-d_6): δ 8.62 (s, 1H), 7.99−7.96 (m, 1H), 7.82−7.71 (m, 2H), 7.70−7.67 (m, 1H), 7.33−7.25 (m, J = 9.3, 2.2 Hz, 1H), 7.11−7.04 (m, 2H). ^{13}C NMR (101 MHz, DMSO-d_6): δ 162.6, 162.3 (dd, $^{1}J_{C,F}$ = 247.8, $^{3}J_{C,F}$ = 13.5 Hz), 156.7 (t, $^{2}J_{C,F}$ = 23.8 Hz), 152.1, 150.8, 142.9 (t, $^{3}J_{C,F}$ = 9.8 Hz), 139.1, 134.0, 132.0 (d, $^{3}J_{C,F}$ = 6.6 Hz), 131.6 (d, $^{2}J_{C,F}$ = 18.5 Hz), 130.9, 129.1, 113.2 (dd, $^{2}J_{C,F}$ = 25.8, $^{2}J_{C,F}$ = 18.1 Hz), 103.6 (td, $^{2}J_{C,F}$ = 25.7, $^{2}J_{C,F}$ = 15.2 Hz). ^{19}F NMR (376 MHz, DMSO): δ 54.04−53.9 (m). Calcd for $C_{16}H_8F_2N_4O$ (310.26): C, 61.94; H, 2.60; N, 18.06. Found: C, 62.11; H, 2.62; N, 18.00.

General Procedure for the Synthesis of Dibenzo[*f,h*]-[1,2,5]oxadiazolo[3,4-*b*]quinoxaline Derivatives (7a−7h). Corresponding 5-([1,1′-biphenyl]-2-yl)-[1,2,5]-oxadiazolo[3,4-*b*]pyrazine derivatives **5a−5h** (0.5 mmol) were dissolved in CF_3COOH (3 mL). The resulting mixture was stirred for 3 h at room temperature; the precipitate formed was filtered off, washed with MeCN (3 × 3 mL), and dried. The obtained 9,13-dihydrodibenzo[*f,h*][1,2,5]oxadiazolo[3,4-*b*]quinoxaline derivatives **6a−6h** were analyzed and further oxidized by the addition of the solution of NaOH (112 mg, 2.0 mmol, 4 equiv) and $K_3Fe(CN)_6$ (329 mg, 1.0 mmol, 2 equiv) in the mixture of EtOH/H_2O (1:5, v/v). The resulting mixture was stirred for 24 h at room temperature and diluted with H_2O (10 mL), and a precipitate was formed and filtered off. The residue was purified by flash column chromatography with CH_2Cl_2 as an eluent to afford the desired dibenzo[*f,h*][1,2,5]-oxadiazolo[3,4-*b*]quinoxaline derivatives (**7a−7h**).

*9,13-Dihydrodibenzo[f,h][1,2,5]oxadiazolo[3,4-b]-quinoxaline (**6a**).* Yield: 130 mg, 95%, white powder. mp 228 °C. ^{1}H NMR (400 MHz, DMSO-d_6): δ 9.95 (s, 2H), 8.77 (d, J = 8.2 Hz, 2H), 8.21 (d, J = 8.2 Hz, 2H), 7.68−7.64 (m, 2H), 7.60−7.57 (m, 2H). ^{13}C NMR (101 MHz, DMSO-d_6): δ 148.0, 127.2, 126.6, 125.1, 123.2, 122.9, 120.5, 118.1. Calcd for $C_{16}H_{10}N_4O$ (274.28): C, 70.06; H, 3.68; N, 20.43. Found: C, 70.15; H, 3.79; N, 20.44.

*2-(tert-Butyl)-9,13-dihydrodibenzo[f,h][1,2,5]oxadiazolo-[3,4-b]quinoxaline (**6b**).* This substance could not be isolated in its pure form.

*1,2,3-Trimethoxy-9,13-dihydrodibenzo[f,h][1,2,5]-oxadiazolo[3,4-b]quinoxaline (**6c**).* Yield: 170 mg, 93%, white powder. mp 221 °C. ^{1}H NMR (500 MHz, DMSO-d_6): δ 9.80 (s, 1H), 9.69 (s, 1H), 8.74 (d, J = 8.3 Hz, 1H), 8.12 (d, J = 8.3 Hz, 1H), 8.03 (s, 1H), 7.64−7.59 (m, 1H), 7.57−7.51 (m, J = 7.5 Hz, 1H), 4.04 (s, 3H), 3.97 (s, 3H), 3.91 (s, 3H). ^{13}C NMR (126 MHz, DMSO-d_6): δ 151.5, 148.5, 147.9, 147.1, 142.2, 127.2, 125.6, 124.9, 124.4, 123.9, 122.6, 120.2, 118.2, 116.7, 111.2, 101.5, 62.5, 60.8, 56.1. Calcd for $C_{19}H_{16}N_4O_4$

https://dx.doi.org/10.1021/acsomega.0c00479
ACS Omega 2020, 5, 8200−8210

(364.36): C, 62.63; H, 4.43; N, 15.38. Found: C, 62.59; H, 4.55; N, 15.38.

*4-Fluoro-9,13-dihydrodibenzo[f,h][1,2,5]oxadiazolo[3,4-b]quinoxaline (**6d**).* This substance could not be isolated in its pure form.

*3-Fluoro-9,13-dihydrodibenzo[f,h][1,2,5]oxadiazolo[3,4-b]quinoxaline (**6e**).* Yield: 130 mg, 89%, white powder. mp 245 °C. ^{1}H NMR (400 MHz, DMSO-d_6): δ 9.96 (s, 1H), 9.90 (s, 1H), 8.72 (d, J = 8.2 Hz, 1H), 8.54 (dd, J = 11.5, 2.4 Hz, 1H), 8.23 (dd, J = 9.2, 5.6 Hz, 1H), 8.18 (d, J = 8.3 Hz, 1H), 7.69−7.64 (m, J = 7.5 Hz, 1H), 7.59−7.50 (m, 2H). ^{13}C NMR (101 MHz, DMSO-d_6): δ 156.0 (d, $^1J_{C,F}$ = 242.3 Hz), 148.0 (d, $^4J_{C,F}$ = 3.5 Hz), 128.4 (d, $^3J_{C,F}$ = 8.3 Hz), 127.8, 125.9 (d, $^4J_{C,F}$ = 4.0 Hz), 125.0, 123.8, 123.4, 123.2, 123.1, 120.4 (d, $^3J_{C,F}$ = 10.6 Hz), 119.8, 118.1, 117.7 (d, J = 2.3 Hz), 115.9 (dd, $^2J_{C,F}$ = 23.7, $^4J_{C,F}$ = 4.3 Hz), 108.40 (dd, $^2J_{C,F}$ = 22.6, $^4J_{C,F}$ = 3.2 Hz).^{19}F NMR (376 MHz, DMSO-d_6): δ 47.05 (ddd, J = 11.5, 8.1, 5.7 Hz). Calcd for $C_{16}H_9FN_4O$ (292.27): C, 65.75; H, 3.10; N, 19.17. Found: C, 65.63; H, 3.14; N, 19.19.

*2-Fluoro-9,13-dihydrodibenzo[f,h][1,2,5]oxadiazolo[3,4-b]quinoxaline (**6f**).* Yield: 84 mg, 56%, white powder. mp 267 °C. ^{1}H NMR (400 MHz, DMSO-d_6): δ 10.02 (s, 1H), 9.86 (s, 1H), 8.82 (dd, J = 9.2, 5.9 Hz, 1H), 8.72 (d, J = 8.0 Hz, 1H), 8.20 (d, J = 8.1 Hz, 1H), 8.01 (dd, J = 11.7, 2.4 Hz, 1H), 7.68−7.56 (m, 2H), 7.43 (td, J = 9.0, 2.4 Hz, 1H). ^{13}C NMR (101 MHz, DMSO-d_6): δ 161.4 (d, $^1J_{C,F}$ = 243.5 Hz), 147.9 (d, $^4J_{C,F}$ = 3.2 Hz), 127.0, 126.4, 126.2 (d, $^3J_{C,F}$ = 9.3 Hz), 125.5, 124.4 (d, $^3J_{C,F}$ = 9.3 Hz), 123.4, 123.4, 123.2, 122.4, 120.5, 119.5, 117.7 (d, $^4J_{C,F}$ = 3.7 Hz), 113.5 (d, $^2J_{C,F}$ = 23.6 Hz), 105.4 (d, $^2J_{C,F}$ = 24.0 Hz). ^{19}F NMR (471 MHz, DMSO-d_6): δ 49.61−49.55 (m). Calcd for $C_{16}H_9FN_4O$ (292.27): C, 65.75; H, 3.10; N, 19.17. Found: C, 65.73; H, 3.21; N, 19.37.

*2,4-Difluoro-9,13-dihydrodibenzo[f,h][1,2,5]oxadiazolo-[3,4-b]quinoxaline (**6g**).* This substance was not detected in the reaction mixture by ^{1}H NMR.

*1,3-Difluoro-9,13-dihydrodibenzo[f,h][1,2,5]oxadiazolo-[3,4-b]quinoxaline (**6h**).* Yield: 120 mg, 77%, white powder. mp 231 °C. ^{1}H NMR (400 MHz, DMSO-d_6): δ 9.96 (s, 1H), 9.07 (d, J = 10.9 Hz, 1H), 8.75 (d, J = 8.1 Hz, 1H), 8.50 (dd, J = 11.0, 1.4 Hz, 1H), 8.21 (d, J = 8.2 Hz, 1H), 7.72 (td, J = 8.0, 0.7 Hz, 1H), 7.64−7.53 (m, 1H). The ^{13}C NMR spectrum cannot be correctly described in view of the extremely low solubility of **6h** in common organic solvents. ^{19}F NMR (376 MHz, DMSO): δ 53.76 (ddd, J = 14.3, 11.2, 7.4 Hz, 1F), 49.51−49.44 (m, 1F). Calcd for $C_{16}H_8F_2N_4O$ (310.26): C, 61.94; H, 2.60; N, 18.06. Found: C, 61.83; H, 2.72; N, 18.12.

*Dibenzo[f,h][1,2,5]oxadiazolo[3,4-b]quinoxaline (**7a**).* Yield: 170 mg, 73%, red powder. mp 281 °C. ^{1}H NMR (400 MHz, DMSO-d_6): δ 8.31 (d, J = 8.0 Hz, 2H), 8.03 (dd, J = 7.7, 1.2 Hz, 2H), 7.79 (td, J = 8.0, 1.2 Hz, 2H), 7.56−7.52 (m, 2H). ^{13}C NMR (101 MHz, DMSO-d_6): δ 152.0, 151.6, 134.0, 133.4, 129.2, 128.7, 127.8, 124.2. Calcd for $C_{16}H_8N_4O$ (272.27): C, 70.58; H, 2.96; N, 20.58. Found: C, 70.46; H, 2.91; N, 20.41.

*2-(tert-Butyl)dibenzo[f,h][1,2,5]oxadiazolo[3,4-b]-quinoxaline (**7b**).* Yield: 157 mg, 96%, red powder. mp 248 °C. ^{1}H NMR (400 MHz, $CDCl_3$): δ 9.15 (s, 1H), 9.07 (d, J = 8.1 Hz, 1H), 8.29 (d, J = 8.1 Hz, 1H), 8.24 (d, J = 8.4 Hz, 1H), 7.86 (dd, J = 8.5, 2.0 Hz, 1H), 7.81−7.76 (m, J = 7.6 Hz, 1H), 7.65−7.59 (m, J = 7.6 Hz, 1H), 1.52 (s, 9H). ^{13}C NMR (101 MHz, $CDCl_3$): δ 152.6, 151.8, 151.7, 151.4, 151.4, 133.8, 133.7, 131.5, 131.2, 128.7, 128.6, 128.6, 128.5, 125.0, 123.3, 123.2, 35.2, 31.2. Calcd for $C_{20}H_{16}N_4O$ (328.28): C, 73.15; H, 4.91; N, 17.06. Found: C, 73.18; H, 4.90; N, 17.16.

*1,2,3-Trimethoxydibenzo[f,h][1,2,5]oxadiazolo[3,4-b]-quinoxaline (**7c**).* Yield: 124 mg, 69%, red powder. mp 259 °C. ^{1}H NMR (400 MHz, $CDCl_3$): δ 9.13 (dd, J = 8.1, 1.1 Hz, 1H), 8.23 (d, J = 8.2 Hz, 1H), 7.83−7.77 (m, 1H), 7.68−7.62 (m, 2H), 4.17 (s, 6H), 4.06 (s, 3H). ^{13}C NMR (101 MHz, $CDCl_3$): δ 157.7, 156.9, 151.5, 151.1, 150.9, 150.1, 145.0, 133.7, 133.4, 131.4, 129.2, 128.73, 128.65, 123.3, 117.5, 102.6, 61.3, 61.1, 56.2. Calcd for $C_{19}H_{14}N_4O_4$ (362.35): C, 62.98; H, 3.89; N, 15.46. Found: C, 62.99; H, 4.14; N, 15.44.

*4-Fluorodibenzo[f,h][1,2,5]oxadiazolo[3,4-b]quinoxaline (**7d**).* Yield: 122 mg, 84%, orange powder. mp 252 °C. ^{1}H NMR (400 MHz, $CDCl_3$): δ 9.25 (d, J = 7.7 Hz, 1H), 9.09 (d, J = 6.8 Hz, 1H), 8.86 (d, J = 5.0 Hz, 1H), 7.89−7.84 (m, 1H), 7.76−7.70 (m, 1H), 7.69−7.56 (m, 2H). The ^{13}C NMR spectrum cannot be correctly described in view of the extremely low solubility of **7d** in common organic solvents.^{19}F NMR (471 MHz, $CDCl_3$): δ 53.53 (dt, J = 13.4, 4.2 Hz). Calcd for $C_{16}H_7FN_4O$ (290.26): C, 66.21; H, 2.43; N, 19.30. Found: C, 66.50; H, 2.34; N, 19.43.

*3-Fluorodibenzo[f,h][1,2,5]oxadiazolo[3,4-b]quinoxaline (**7e**).* Yield: 135 mg, 93%, orange powder. mp 282 °C. ^{1}H NMR (400 MHz, $CDCl_3$): δ 9.24−9.19 (m, 2H), 8.30 (d, J = 8.2 Hz, 1H), 8.04 (dd, J = 10.2, 2.4 Hz, 1H), 7.91−7.85 (m, 1H), 7.77−7.73 (m, 1H), 7.41 (ddd, J = 9.0, 7.7, 2.5 Hz, 1H). ^{13}C NMR (101 MHz, $CDCl_3$): cannot be correctly described in view of the extremely low solubility of **7e** in common organic solvents. ^{19}F NMR (376 MHz, $CDCl_3$): δ 58.73 (ddd, J = 10.3, 7.5, 6.2 Hz). Calcd for $C_{16}H_7FN_4O$ (290.26): C, 66.21; H, 2.43; N, 19.30. Found: C, 66.23; H, 2.55; N, 19.34.

*2-Fluorodibenzo[f,h][1,2,5]oxadiazolo[3,4-b]quinoxaline (**7f**).* Yield: 114 mg, 78%, orange powder. mp 256 °C. ^{1}H NMR (500 MHz, $CDCl_3$): δ 9.18 (dd, J = 8.1, 0.8 Hz, 1H), 8.83 (dd, J = 9.5, 2.8 Hz, 1H), 8.39 (dd, J = 8.9, 5.1 Hz, 1H), 8.32 (d, J = 8.1 Hz, 1H), 7.87−7.83 (m, 1H), 7.72−7.68 (m, 1H), 7.57 (ddd, J = 9.0, 7.5, 2.8 Hz, 1H). ^{13}C NMR (101 MHz, $CDCl_3$): δ 163.0 (d, $^1J_{C,F}$ = 250.9 Hz), 151.6, 151.5, 151.3, 150.6 (d, $^4J_{C,F}$ = 3.1 Hz), 133.9, 133.1, 131.2 (d, $^3J_{C,F}$ = 8.1 Hz), 130.3 (d, $^4J_{C,F}$ = 3.0 Hz), 129.0, 128.7, 128.6, 125.8 (d, $^3J_{C,F}$ = 8.1 Hz), 123.4, 121.6 (d, $^2J_{C,F}$ = 22.9 Hz), 114.3 (d, $^2J_{C,F}$ = 23.7 Hz). ^{19}F NMR (471 MHz, $CDCl_3$): δ 51.23 (ddd, J = 9.5, 7.5, 5.1 Hz). Calcd for $C_{16}H_7FN_4O$ (290.26): C, 66.21; H, 2.43; N, 19.30. Found: C, 66.29; H, 2.47; N, 19.24.

*2,4-Difluorodibenzo[f,h][1,2,5]oxadiazolo[3,4-b]-quinoxaline (**7g**).* This substance was not detected in the reaction mixture by ^{1}H NMR.

*1,3-Difluorodibenzo[f,h][1,2,5]oxadiazolo[3,4-b]-quinoxaline (**7h**).* Yield: 118 mg, 77%, orange powder. mp 269 °C. ^{1}H NMR (400 MHz, $CDCl_3$): δ 9.24 (dd, J = 8.1, 1.2 Hz, 1H), 8.32 (d, J = 8.2 Hz, 1H), 8.01−7.96 (m, 1H), 7.94−7.89 (m, 1H), 7.80 (td, J = 7.7, 1.0 Hz, 1H), 7.23 (ddd, J = 11.5, 8.2, 2.5 Hz, 1H). The ^{13}C NMR spectrum cannot be correctly described in view of the extremely low solubility in common organic solvents. ^{19}F NMR (471 MHz, $CDCl_3$): δ 66.81 (dd, J = 14.9, 11.8 Hz, 1F), 62.03 (ddd, J = 15.7, 9.8, 8.3 Hz, 1F). Calcd for $C_{16}H_6F_2N_2O$ (308.25): C, 62.34; H, 1.96; N, 18.18. Found: C, 62.47; H, 1.98; N, 18.16.

https://dx.doi.org/10.1021/acsomega.0c00479
ACS Omega 2020, 5, 8200−8210

■ ASSOCIATED CONTENT

Supporting Information

The Supporting Information is available free of charge at https://pubs.acs.org/doi/10.1021/acsomega.0c00479.

Compound characterization checklist (XLS)
Crystallographic data for **7h** (CIF)
Cyclic voltammograms of compounds; UV−vis absorption spectra of compounds **7a**−**7f** and **7h**; and ^{1}H, ^{13}C, and ^{19}F NMR spectra for all new compounds (PDF)

■ AUTHOR INFORMATION

Corresponding Author

Egor V. Verbitskiy − *Postovsky Institute of Organic Synthesis, Ural Branch of the Russian Academy of Sciences, Ekaterinburg 620108, Russia; Ural Federal University, Ekaterinburg 620002, Russia;* orcid.org/0000-0002-9613-8738; Email: Verbitsky@ios.uran.ru

Authors

Yuriy A. Kvashnin − *Postovsky Institute of Organic Synthesis, Ural Branch of the Russian Academy of Sciences, Ekaterinburg 620108, Russia*

Oleg S. Eltsov − *Ural Federal University, Ekaterinburg 620002, Russia*

Pavel A. Slepukhin − *Postovsky Institute of Organic Synthesis, Ural Branch of the Russian Academy of Sciences, Ekaterinburg 620108, Russia; Ural Federal University, Ekaterinburg 620002, Russia*

Alexey R. Tameev − *Postovsky Institute of Organic Synthesis, Ural Branch of the Russian Academy of Sciences, Ekaterinburg 620108, Russia; Frumkin Institute of Physical Chemistry and Electrochemistry of the Russian Academy of Sciences, Moscow 119071, Russia*

Natalia V. Nekrasova − *Frumkin Institute of Physical Chemistry and Electrochemistry of the Russian Academy of Sciences, Moscow 119071, Russia*

Gennady L. Rusinov − *Postovsky Institute of Organic Synthesis, Ural Branch of the Russian Academy of Sciences, Ekaterinburg 620108, Russia; Ural Federal University, Ekaterinburg 620002, Russia*

Jean-Michel Nunzi − *Department of Physics, Engineering Physics and Astronomy, Department of Chemistry, 90 Bader Lane, Queens University, Kingston, Ontario K7L-3N6, Canada;* orcid.org/0000-0001-5490-4273

Oleg N. Chupakhin − *Postovsky Institute of Organic Synthesis, Ural Branch of the Russian Academy of Sciences, Ekaterinburg 620108, Russia; Ural Federal University, Ekaterinburg 620002, Russia;* orcid.org/0000-0002-1672-2476

Valery N. Charushin − *Postovsky Institute of Organic Synthesis, Ural Branch of the Russian Academy of Sciences, Ekaterinburg 620108, Russia; Ural Federal University, Ekaterinburg 620002, Russia*

Complete contact information is available at: https://pubs.acs.org/10.1021/acsomega.0c00479

Notes

The authors declare no competing financial interest.

■ ACKNOWLEDGMENTS

The research was financially supported by the Russian Science Foundation (project no. 18-13-00409). Y.A.K would like to acknowledge the financial support for the part of the synthetic section from the Russian Foundation for Basic Research (research project no. 18-33-00103-mol_a). The authors are grateful to Grigory A. Kim for carrying out the DFT calculations, which were performed by using "Uran" supercomputer of the Institute of Mathematics and Mechanics of the Ural Branch of the Russian Academy of Sciences. NMR experiments were carried out by using equipment of the Center for Joint Use "Spectroscopy and Analysis of Organic Compounds" at the Postovsky Institute of Organic Synthesis of the Ural Branch of the Russian Academy of Sciences.

■ REFERENCES

(1) (a) Bendikov, M.; Wudl, F.; Perepichka, D. F. Tetrathiafulvalenes, oligoacenenes, and their buckminsterfullerene derivatives: The brick and mortar of organic electronics. *Chem. Rev.* **2004**, *104*, 4891−4946. (b) Anthony, J. E. Functionalized acenes and heteroacenes for organic electronics. *Chem. Rev.* **2006**, *106*, 5028−5048. (c) Wang, C.; Dong, H.; Hu, W.; Liu, Y.; Zhu, D. Semiconducting π-conjugated systems in field-effect transistors: A material odyssey of organic electronics. *Chem. Rev.* **2012**, *112*, 2208−2267. ((d)) Lakshminarayana, A. N.; Chi, C. *Polycyclic Arenes and Heteroarenes: Synthesis, Properties, and Applications*; Miao, Q., Ed.; Wiley-VCH: Weinheim, 2015; p 225; (e) Stępień, M.; Gońka, E.; Żyła, M.; Sprutta, N. Heterocyclic nanographenes and other polycyclic heteroaromatic compounds: Synthetic routes, properties, and applications. *Chem. Rev.* **2016**, *117*, 3479−3716.

(2) Verbitskiy, E. V.; Rusinov, G. L.; Charushin, V. N. Diazatriphenylenes and their thiophene analogues: synthesis and applications. *ARKIVOC* **2017**, *I*, 356−401.

(3) (a) Gasco, A.; Ruà, G.; Menziani, E.; Nano, G. M.; Tappi, G. Studies in the chemistry of 1,2,5-oxadiazole. I. Synthesis of some furazanopyrazines from 3,4-diamino-1,2,5-oxadiazole. *J. Heterocycl. Chem.* **1969**, *6*, 769−770. ((b)) Ishibashi, S.; Fujio, K. Photoconductive coatings and their use as electrophotographic photoconductors. Patent JP 64002053 A, 1989.

(4) Verbitskiy, E. V.; Kvashnin, Y. A.; Slepukhin, P. A.; Kuchin, A. V.; Rusinov, G. L.; Chupakhin, O. N.; Charushin, V. N. Reactions of pyrazinium salts with phenols:from σ^{H}-adducts to S_N^H products and transformations into benzo[b]furans. *Russ. Chem. Bull.* **2011**, *60*, 919−928.

(5) Chung, D. D. L. Review graphite. *J. Mater. Sci.* **2002**, *37*, 1475−1489.

(6) Wu, J.; Pisula, W.; Müllen, K. Graphenes as potential material for electronics. *Chem. Rev.* **2007**, *107*, 718−747.

(7) Verbitskiy, E. V.; Dinastiya, E. M.; Baranova, A. A.; Eltsov, O. S.; Rusinov, G. L.; Chupakhin, O. N.; Charushin, V. N. Synthesis of dithienoquinazolines from pyrimidines via intramolecular nucleophilic aromatic substitution of hydrogen. *Chem. Heterocycl. Compd.* **2017**, *53*, 1156−1160.

(8) Costa, J. C. S.; Taveira, R. J. S.; Lima, C. F. R. A. C.; Mendes, A.; Santos, L. M. N. B. F. Optical band gaps of organic semiconductor materials. *Opt. Mater.* **2016**, *58*, 51−60.

(9) Neese, F. The ORCA program system. *Wiley Interdiscip. Rev.: Comput. Mol. Sci.* **2011**, *2*, 73−78.

(10) Stolka, M.; Yanus, J. F.; Pai, D. M. Hole transport in solid solutions of a diamine in polycarbonate. *J. Phys. Chem.* **1984**, *88*, 4707−4714.

(11) Tameev, A. R.; He, Z.; Milburn, G. H. W.; Kozlov, A. A.; Vannikov, A. V.; Danel, A.; Tomasik, P. *Appl. Phys. Lett.* **2000**, *77*, 322−324.

(12) Tameev, A. R.; He, Z.; Milburn, G. H. W.; Kozlov, A. A.; Vannikov, A. V.; Puchala, A.; Rasala, D. Electron drift mobility in polystyrene doped with bispyrazolopyridine derivatives. *Appl. Phys. Lett.* **2002**, *81*, 969−971.

(13) Coropceanu, V.; Cornil, J.; da Silva Filho, D. A.; Olivier, Y.; Silbey, R.; Brédas, J.-L. Charge transport in organic semiconductors. *Chem. Rev* **2007**, *107*, 926−952.

(14) Novikov, S. V.; Vannikov, A. V. Cluster structure in the distribution of the electrostatic potential in a lattice of randomly oriented dipoles. *J. Phys. Chem.* **1995**, *99*, 14573−14576.
(15) Novikov, S. V.; Dunlap, D. H.; Kenkre, V. M.; Parris, P. E.; Vannikov, A. V. Essential role of correlations in governing charge transport in disordered organic materials. *Phys. Rev. Lett.* **1998**, *81*, 4472−4475.
(16) Aukštuolis, A.; Girtan, M.; Mousdis, G. A.; Mallet, R.; Socol, M.; Rasheed, M.; Stanculescu, A. Measurement of charge carrier mobility in perovskite nanowire films by photo-CELIV method. *Proc. Rom. Acad. Ser. A, Rom.Acad.* **2017**, *18*, 34−41.
(17) Poplavskyy, D.; Nelson, J. Nondispersive hole transport in amorphous films of methoxy-spirofluorene-arylamine organic compound. *J. Appl. Phys.* **2003**, *93*, 341−346.
(18) Dolomanov, O. V.; Bourhis, L. J.; Gildea, R. J.; Howard, J. A. K.; Puschmann, H. *OLEX2*: a complete structure solution, refinement and analysis program. *J. Appl. Crystallogr.* **2009**, *42*, 339−341.
(19) Palatinus, L.; Chapuis, G. *SUPERFLIP* − a computer program for the solution of crystal structures by charge flipping in arbitrary dimensions. *J. Appl. Crystallogr.* **2007**, *40*, 786−790.
(20) Cardona, C. M.; Li, W.; Kaifer, A. E.; Stockdale, D.; Bazan, G. C. Electrochemical considerations for determining absolute frontier orbital energy levels of conjugated polymers for solar cell applications. *Adv. Mater.* **2011**, *23*, 2367−2371.
(21) Namazian, M.; Lin, C. Y.; Coote, M. L. Benchmark calculations of absolute reduction potential of ferricinium/ferrocene couple in nonaqueous solutions. *J. Chem. Theory Comput.* **2010**, *6*, 2721−2725.
(22) Mozer, A. J.; Sariciftci, N. S.; Pivrikas, A.; Österbacka, R.; Juška, G.; Brassat, L.; Bässler, H. Charge carrier mobility in regioregular poly(3-hexylthiophene) probed by transient conductivity techniques: A comparative study. *Phys. Rev. B* **2005**, *71*, No. 035214.
(23) Irgashev, R. A.; Kazin, N. A.; Makarova, N. I.; Dorogan, I. V.; Malov, V. V.; Tameev, A. R.; Rusinov, G. L.; Metelitsa, A. V.; Minkin, V. I.; Charushin, V. N. Synthesis and properties of new π-conjugated imidazole/carbazole structures. *Dyes Pigm.* **2017**, *141*, 512−520.
(24) Malov, V. V.; Ghosh, T.; Nair, V. C.; Maslov, M. M.; Katin, K. P.; Unni, K. N. N.; Tameev, A. R. Hole mobility in thieno[3,2-*b*]thiophene oligomers. *Mendeleev commun.* **2019**, *29*, 218−219.

https://dx.doi.org/10.1021/acsomega.0c00479
ACS Omega 2020, 5, 8200−8210